Time-dependent equations governing the shape of a two-dimensional liquid curtain, Part 2: Experiment

Andrew Clarke
Kodak European R&D, Headstone Drive, Harrow HA1 4TY, United Kingdom

Steven J. Weinstein and Alice G. Moon
Eastman Kodak Company, Rochester, New York 14652-3701

Elizabeth A. Simister
Kodak European R&D, Headstone Drive, Harrow HA1 4TY, United Kingdom

(Received 25 April 1997; accepted 18 August 1997)

In Part I of this paper, two governing equations have been derived that describe the shape of a falling liquid sheet (a curtain) subjected to ambient pressure disturbances. These equations are termed varicose and sinuous. The varicose equation governs thickness variations in the curtain, for which the two air–liquid interfaces move exactly out of phase. The sinuous equation governs the deflection of the curtain centreline, i.e., the two air–liquid interfaces move in phase such that the local thickness of the liquid is preserved. To the order of the approximations used, the theory presented in Part 1 indicates that pressure disturbances invoke a sinuous curtain deflection with no varicose contribution. In Part 2 of this paper, the sinuous equation is verified by means of a localised pressure disturbance induced by an electrostatic field. After initiation, the propagation of this disturbance is followed and the shape of the air liquid interface is measured using a laser reflection technique. Both the generation and detection of the disturbance are non-contacting and therefore allow a precise verification of the equation. [S1070-6631(97)02312-X]

I. INTRODUCTION

In Part 1 of this paper, the problem of a planar liquid sheet (a curtain) falling under the influence of gravity and subjected to ambient time-dependent pressure disturbances is considered theoretically. Approximate equations are derived which govern the shape of the liquid curtain under conditions of potential flow by linearizing the full equation set about the undisturbed flow in the curtain. In the absence of disturbances, it is shown that the curtain speed, u, satisfies

$$u=[V^2+2gx]^{1/2}, \tag{1a}$$

where x is the distance down the curtain (Figure 1), V is the speed at $x=0$, and g is acceleration due to gravity. The local thickness of the curtain, h, is therefore given in terms of the constant volumetric flow per unit width in the curtain, q, as

$$h=\frac{q}{u}. \tag{1b}$$

In its undisturbed state, note that the curtain flow and shape are symmetrical about the line $y=0$ shown in Figure 1. The result (1) is an approximation to the full potential flow equations under the assumption that the curtain is long and thin, as characterised by small values of the parameter ε defined as

$$\varepsilon=\frac{qg}{V^3}. \tag{2}$$

In reality, the velocity profile across the curtain is slightly curved, but these effects are of $O(\varepsilon^2)$ as demonstrated in Part 1 of this paper. The neglect of viscosity concomitant with potential flow is justified by the large magnitude of the appropriate Reynolds number, the inverse of which is given in equation (2c) of Part 1.

After linearizing the time-dependent potential flow equation about the approximated base flow, two distinct governing equations arise. The first equation governs the average location of the front and back interfaces, i.e., the location of the curtain centreline parameterized as $y=F'(x,t)$ (see Figure 1 for the co-ordinate system). Thus the curtain response is sinuous, in that the local thickness given by (1b) is unaltered even as the curtain deflects. The sinuous equation is given by

$$\left(\frac{\partial}{\partial t}+g\frac{\partial}{\partial u}\right)^2 F'-\frac{2\sigma g^2}{\rho q}\frac{\partial}{\partial u}\left[\frac{1}{u}\frac{\partial F'}{\partial u}\right]=\frac{(P_2-P_1)u}{\rho q}. \tag{3}$$

In (3), u is the free-fall speed given by (1a), t is time, σ the constant surface tension of both air–liquid interfaces, and ρ the density. The pressures on the front and back faces of the curtain (corresponding to the right and left sides of the curtain shown in the cross section of Figure 1) are given by P_1 and P_2, respectively. Equation (3) is valid strictly for small curtain deflections, which correspond to small pressure disturbances to the curtain. The second equation which arises governs varicose disturbances to the curtain, i.e. thickness variations, and is independent of any deflection of the curtain centreline. These thickness variations, parameterized as $G'(x,t)$, are governed by the varicose equation

$$\frac{\partial G'}{\partial t}+\frac{\partial(uG')}{\partial x}=0. \tag{4}$$

We note here that the solution for $G'(x,t)$ can be added to the undisturbed thickness h in (1b) to yield the actual thickness of the curtain during a disturbance.

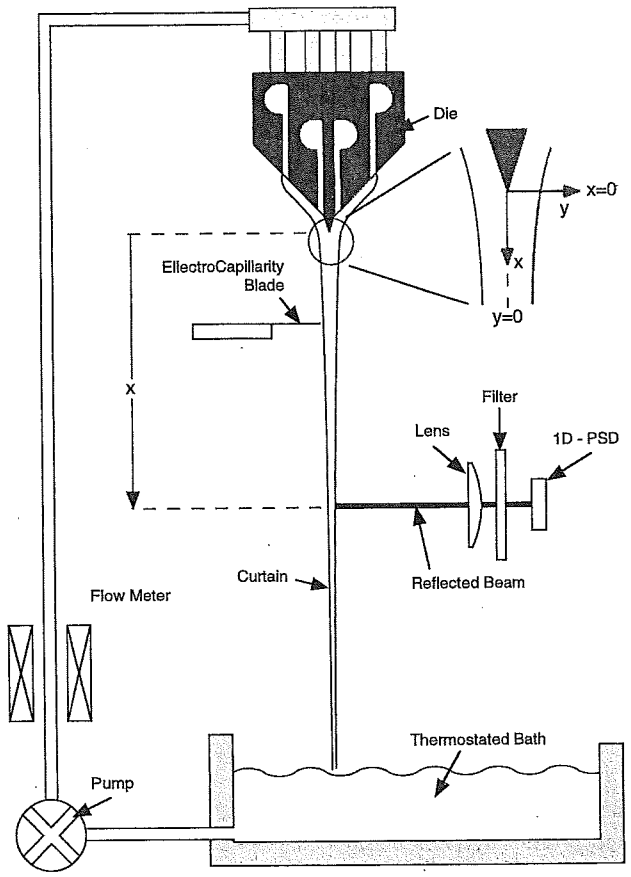

FIG. 1. A schematic diagram of the overall arrangement of the curtain apparatus. A die extrudes a liquid sheet which falls past an electrostatic blade and an optical detection system. The liquid is then recirculated via an in-line flowmeter. The detector is mounted on a rail table allowing it to scan over the full length of the curtain. The x ordinate is measured as the distance down the curtain from the die lip and the y ordinate is measured from the curtain centreline.

In Part 1 of this paper, evidence for the validity of equations (3) and (4) was provided via comparisons with previous literature results. Finnicum *et al.*[1] investigated curtain shapes due to an imposed steady pressure drop via theoretical and experimental means. Their derived equation is identical to the time-independent form of the sinuous equation (3) for small curtain deflections, and is in excellent agreement with experimental results they provide. Ramos[2] derived a varicose equation to describe the shape of viscous liquid curtains, which, in its limiting inviscid form, is demonstrated in Part 1 of this paper to be identical to our equation (4). With the exception of these references, previous studies have focused on wave propagation in the curtain using both theoretical and experimental means.[3–6] In these works, the dispersion relations between frequency, wavelength, and wavegrowth have been investigated in detail. However, none have measured, in a controlled and non-contact fashion, the *shape* of the liquid–air interface as a function of position in the curtain as a wave propagates in the downward direction. Lin and Roberts[4] made detailed measurements of the liquid velocity and of the stationary wave induced by a rod which pierced the curtain. They compared their results to a previous theoretical analysis by Lin.[3] Although these two papers give sufficient detail to predict the position of the stationary wave, they do not consider how the shape of the liquid curtain is affected. In another work by Balbaert *et al.*,[6] the wavelengths of capillary waves induced in the curtain are measured in order to determine the local liquid surface tension. In that study, the waves were induced by a wire laid in the curtain and arranged such that the waves propagate in a direction normal to the curtain flow, i.e., across the curtain. In all these cases, the initial disturbance has been introduced by making contact with the liquid surface. Although this is perhaps the simplest means to generate a disturbance, the liquid flow will inevitably be redistributed and the local velocity field altered in a complex way. There have also been many studies of capillary wave propagation on a static liquid surface,[7–9] and on a liquid flowing down an inclined plane.[10] In these, waves were generated by an electrostatic means, i.e. non-contact, and detected by means of reflected light, again non-contact.

In our work, we are primarily interested in how localised pressure disturbances affect the shape of the curtain. Equation (3) shows an explicit appearance of a pressure drop term, while equation (4) does not; this indicates that to the order of the approximations used, pressure disturbances are coupled directly to the sinuous equation, but not the varicose. The varicose equation is therefore of lesser interest here. In this paper we thus concentrate on the experimental verification of the sinuous equation. In our study, the non-contact methods cited above have been used to disturb the curtain and measure the resulting time-dependent shape. We note here that previous experimental work by Finnicum *et al.*[1] verifies that the time-independent form of the sinuous governing equation (3) is correct, and thus the static case will not be considered here.

II. EXPERIMENT

A. Experimental methods

A two-dimensional liquid curtain is formed by a die consisting of four slots arranged symmetrically about a central plate,[11] Figure 1. This arrangement generates a symmetrically falling curtain irrespective of the flow rate, provided the flow is divided equally between the two faces of the die. In addition, the initial liquid velocity as it leaves the die is low and only weakly dependent on the flow rate. The curtain falls into a trough which collects the liquid so that it may be recirculated. Both the bath and the die are thermostated such that a reasonably constant temperature is achieved throughout the system. The edges of the curtain are anchored using stainless steel rods flushed with water. The water both lubricates the curtain flow and assists in anchoring the curtain, which would otherwise taper under the influence of surface tension to a central stream. The water flush is extracted to waste allowing the majority of the liquid to be recirculated without becoming diluted. This additional water system has been omitted from Figure 1 for clarity.

A time-dependent disturbance is generated on the curtain using an electrostatic field; a thin (125 μm) horizontal blade of width equal to the curtain width (89 mm), is positioned close to the liquid surface and a high voltage is applied. This

method is well known for exciting waves on stationary liquid interfaces,[7] and has also been used for exciting waves on liquid surfaces flowing in a steady state.[10] The electrostatic field exerts an attractive force at the liquid surface proportional to the square of the field strength. Provided the liquid is sufficiently conducting, the electrostatic field will be perpendicular to the liquid surface everywhere and will act as a localised and well defined pressure disturbance (if the liquid were insulating, a much weaker force would be felt). The standard definition of electrostatic pressure, P, gives

$$P=\tfrac{1}{2}\varepsilon_r\varepsilon_0[E(x-x_0)]^2, \tag{5a}$$

where ε_r is relative permittivity, ε_0 is the permittivity of free space, x_0 is the blade position, and $E(x-x_0)$ is the electrostatic field strength as a function of distance along the liquid surface. If the electrostatic blade is considered a semi-infinite plane at potential V assumed to be separated a distance d from the liquid surface (a perpendicular ground plane), then the field strength, $E(x-x_0)$, can be obtained using standard conformal mapping techniques as

$$E(x-x_0)=\frac{2V}{\pi[(x-x_0)^2+d^2]^{1/2}}. \tag{5b}$$

The profile of the pressure disturbance therefore has a Lorentzian shape centered on the blade position with a full width at half maximum of twice the distance of the blade from the liquid surface. With typical values, this gives a disturbance with a peak pressure of approximately 2 Pa and a width of approximately 1 mm. The method therefore provides a well defined and controllable pressure disturbance.

If a sinusoidally oscillating voltage is applied to the blade, a periodic disturbance is generated in the curtain. Since the pressure is proportional to the square of the field and therefore the square of the voltage, it is independent of the sign, and a voltage oscillation at ω will produce a disturbance in the curtain at 2ω, i.e., twice the voltage frequency $[\cos^2(\omega)=0.5*(1+\cos(2\omega))]$. In addition, the maximum amplitude of the disturbance generated by a given voltage on the blade is inversely proportional to the distance between the blade and the curtain (nominally 0.5 mm). Therefore, small air disturbances which disturb the equilibrium position of the curtain relative to the blade can dramatically affect the initial amplitude; hence, the entire apparatus is shielded from random air disturbances by a Perspex box. Figure 2 shows the electronic arrangement of the experiment. A sinusoidal voltage is applied to the blade from a Trek 610c high voltage amplifier driven by the internal oscillator of the lock-in amplifier. Voltage amplitudes in the range 300 V–1200 V were used.

The optical detection system is detailed in Figure 3. Light from a diode laser (LaserMax LFX-250-680-20) passes through a cylindrical concave lens and is reflected from the curtain surface. The lens spreads the laser beam to form a thin horizontal sheet of light. By this means, the detector is made insensitive to the exact alignment of the laser and to any misalignment of the curtain about a vertical axis. The reflected light passes via a cylindrical convex lens and a filter to a position sensitive detector (1D-PSD; Hamamatsu C3683-01 with S3932 photodiode). The purpose of the filter

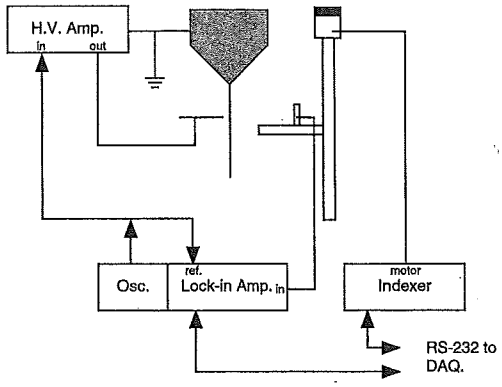

FIG. 2. The electronic arrangement of the experiment. The lock-in amplifier internal oscillator provides a reference signal which is amplified by a Trek high voltage amplifier to drive the electrostatic blade. The lock-in is referenced to 2ω and measures the signal generated by the position sensitive detector (1D-PSD). The rail table and lock-in are both controlled via RS-232 serial lines.

is to remove unwanted room light; although we detect the synchronous signal using a lock-in amplifier and ambient light should therefore not contribute to the signal, it will reduce the dynamic range of the detector. The entire optical system is mounted on a rail table (Parker model 5061415ETLH), driven by a stepper motor (S57-102-MO) and indexer (PDX-13) and can examine the curtain over a 300 mm range below the die exit.

The optical detection system measures the slope of the liquid–air interface. As a disturbance moves past the detector the light beam will be deflected up and down; this deflection is registered as a change in position of the beam as it falls on the position sensitive detector. If the sensitivity of the detector is Φ V per unit length and the distance between the curtain and the detector is r, the signal measured will be

$$s=2\Phi r\frac{\partial F'}{\partial x}. \tag{6}$$

With our optical arrangement, the overall detection sensitivity ($2\Phi r$) becomes 0.104 V/mrad. Typically, waves in our experiment with amplitude 3 μm [approx. $h/100$; see eq.

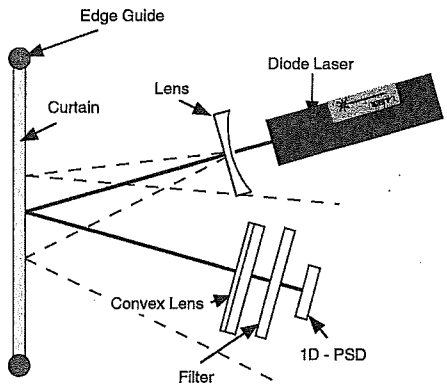

FIG. 3. A schematic of the optical detection system. A diode laser generates a beam of light which is spread by a cylindrical concave lens. The reflected light is detected by a 1D position sensitive detector and the deflection is measured.

(1b)] and wavelength 2 mm, have a maximum slope of approximately 9 mrad and thus a signal of 0.9 V. We are thus able to detect small perturbations and are able to work well within the linear regime of the system.

The entire experiment is controlled by computer via RS-232 serial lines using software writter with LabVIEW.[12] The rail table is driven to the required location where the signal is measured. The lock-in amplifier performs the required A-to-D conversions and the measurement of amplitude and phase are read and stored by the software. This process is repeated for as many data points as are required.

Aqueous glycerol was used for all the experiments presented in this paper. The temperature was maintained at 25 °C. During the course of the experiments samples were taken for surface tension and density measurements to ensure an accurate value of the Weber number [see equation (7d) for definition] could be obtained. The surface tension was measured using a Wilhelmy plate and sensitive balance and the density with a PAAR DMA 48 density meter. In addition, accurate values for the volumetric flow rate were required and were obtained using an *in-situ* magnetic flowmeter (Altometer SC 100 AS). Typical values of surface tension, density, and viscosity were, respectively, 66.0 mN m^{-1}, 1.2105 g cm^{-3}, and 56.2 mPa s, respectively. The viscosity was measured using a Bohlin CS rheometer. These values varied by only a few percent over the course of the experiments, but even so, were obtained for each dataset.

In order to check that the imposed disturbance was within the linear regime, two independent experiments were performed. First, the signal amplitude was measured over the electrostatic blade as a function of voltage on the blade. Provided the amplitude doubled when the electrostatic force was doubled (i.e., voltage multiplied by $\sqrt{2}$) the system was behaving linearly. A second check was provided by a spectrum analyser which measured the signal power spectrum at the chosen excitation voltage. If no harmonics were observed then the system was certainly within the linear regime.

B. Interpretation of the sinuous governing equation

To facilitate the comparison between experiment and theory, the effect of the electrostatic pressure disturbance [eq. (5)] needs to be incorporated into the sinuous governing equation (3). Let us denote a location within the curtain below the electrostatic blade as $x=x_0$, and denote the corresponding velocity at this point as u_0 according to the free-fall formula (1a). Since the electrostatic disturbance itself is applied along a line perpendicular to the flow, we choose to incorporate it into our modelling as boundary conditions applied at $x=x_0$. Consequently, the right-hand side of (3) will be zero, and its effects will be incorporated into the boundary conditions. This choice is made in preference to solving the inhomogeneous equation since equation (5) contains approximations which would preclude precise verification of the governing equation (3). In addition, equation (5) contains the blade to liquid distance, d, which is inherently difficult to measure. The disturbance imparted to the curtain by the blade has an angular frequency ω, and has complex amplitude α. Inspection of (3) indicates that we can therefore look for a solution of the curtain shape in the form

$$\bar{F}' = \bar{\alpha} e^{i\bar{\omega}\bar{t}} \bar{H}'(\bar{u}), \tag{7a}$$

where the overbars denote dimensionless quantities defined as

$$\bar{F}' = \frac{F'V}{q}, \quad \bar{u} = \frac{u}{V}, \quad \bar{t} = \frac{tg}{V}, \quad \bar{\omega} = \frac{\omega V}{g}, \quad \bar{\alpha} = \frac{\alpha V}{q}. \tag{7b}$$

In (7a), all quantities used for scaling are defined in the introduction (Sec. I). Substituting (7b) into the dimensionless version of (3) yields

$$(\bar{u}^2 - 2W\bar{u}) \frac{d^2\bar{H}'}{d\bar{u}^2} + (2W + 2i\bar{\omega}\bar{u}^2) \frac{d\bar{H}'}{d\bar{u}} - \bar{\omega}^2\bar{u}^2\bar{H}' = 0, \tag{7c}$$

where W is the Weber number defined as

$$W = \frac{\sigma}{\rho q V}. \tag{7d}$$

Note that the speed is related to the distance down the curtain according to (1a), which is written in dimensionless form as

$$\bar{u} = [1 + 2\bar{x}]^{1/2}, \text{ where } \bar{x} = \frac{xg}{V^2}. \tag{7e}$$

Inspection of (7c) indicates that two boundary conditions are needed to obtain a well posed problem. These are the complex amplitude and slope at $\bar{u}=\bar{u}_0$. The form given in (7a) lumps the initial amplitude of the curtain deflection at $\bar{u}=\bar{u}_0$ into $\bar{\alpha}$; thus the constraint for $\bar{H}'$ is

$$\bar{H}' = 1, \quad \text{at } \bar{u}=\bar{u}_0. \tag{7f}$$

A slope constraint can be written as

$$\frac{d\bar{H}'}{d\bar{u}} = \beta, \quad \text{at } \bar{u}=\bar{u}_0, \tag{7g}$$

where β is a constant dimensionless parameter. We note here that β is not directly measured in our experiments; rather, we obtain the dimensional slope, $\partial F'/dx$, which is expressed in terms of β as

$$\frac{\partial F'}{\partial x} = \alpha\beta \frac{g}{u_0} e^{i\omega t}, \quad \text{at } x=x_0(\bar{u}=\bar{u}_0). \tag{8}$$

We also note that we did obtain an analytical power series solution to the equation (7c), but found it to be divergent. As a result, equation (7c) was numerically integrated using a standard predictor–corrector method.

III. RESULTS

A. Measurement of curtain velocity

Previous workers[4,5] have measured the free-fall velocity of a liquid curtain by essentially the same method as used here. In all cases the data obtained have been well described by free-fall. In the present case, we have chosen to verify that the liquid is in free-fall and also to estimate the distance from the die lip at which the free-fall description becomes valid. In addition, we obtain an estimate of the velocity at which the liquid leaves the die lip.

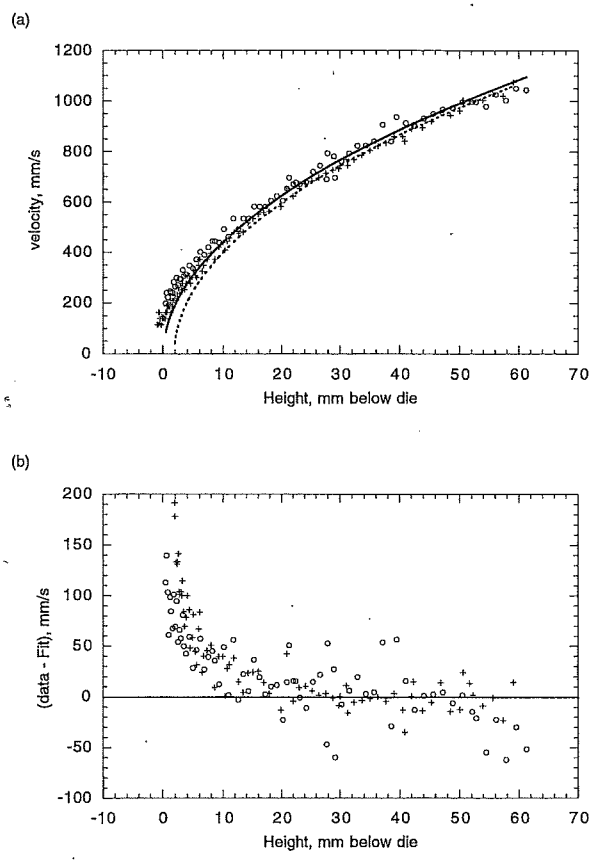

FIG. 4. Liquid velocity as a function of height below the die lip (a) data for two flow rates 5 cm^2/s (O, data; —, fit) and 3.5 cm^2/s (+, data; ---, fit). (b) The difference between measured and fitted free-fall velocity. Note that the velocity is well fitted by the free-fall equation at distances greater than approximately 15 mm from the lip.

Figure 4a shows measurements of the liquid velocity for 60 mm below the die lip, together with the fitted free-fall velocity. These measurements were made by stroboscopically lighting the curtain and measuring particle positions (bubbles induced in the flow) as a function of time. Because of the four slot nature of the die, the bubbles tend to align at positions 1/8, 3/8, 5/8, and 7/8 of the thickness of the curtain and hence the measured velocity close to the die lip will be greater than the average liquid velocity. Our measured velocity is thus systematically higher than the average curtain velocity close to the die lip and therefore more sensitive to deviations from free-fall in this region. Figure 4b shows the difference between a fit of free-fall velocity and that measured. It can be seen that at distances greater than approximately 15 mm from the die the curtain is in free fall. This distance corresponds to approximately four times the initial curtain thickness at the die lip assuming fully developed flow on the die faces. Using these thicknesses, the initial velocity compares well with the calculated average liquid velocity on each face of the die. The velocity measurements therefore verify the base flow equation (1a) and indicate that for our verification of the sinuous equation, we should only excite and measure disturbances at distances greater than 15 mm from the die lip.

B. Measurement of the curtain shape

To compare the predictive capability of equation (3) with experiment, data over a range of flow rate ($2.65\ cm^2/s < q < 4.71\ cm^2/s$) and blade height ($33\ mm < x_0 < 93\ mm$) were obtained. It is convenient to combine these into a local Weber number W_b defined as

$$W_b = \frac{W}{\overline{u}_0} = \frac{\sigma}{\rho q u_0}. \tag{9}$$

The range of W_b in our experiments was thus $0.08 < W_b < 0.26$, where the surface tension and density were independently measured and curtain velocity calculated at $x = x_0$ as described above. Note, for this range of conditions, the value of ε based on the liquid velocity at the blade location [i.e., V in equation (2) is taken as u_0] is $\varepsilon < 0.01$, and therefore higher order corrections to equations (1) and (3) [which are of $O(\varepsilon^2)$] are negligible and the assumption that the curtain is long and thin is valid. Furthermore, a range of frequencies, ω, were considered, 251 rad s^{-1} (40 Hz), 440 rad s^{-1} (70 Hz), and 691 rad s^{-1} (110 Hz). The estimated standard error on the local Weber number is $\pm 3.5\%$, which arises primarily from the estimated error in the liquid velocity (see Figure 4).

In principle, it is possible to measure the initial slope directly from the data and to use this value as the boundary condition which, together with the measured Weber number, leaves only the absolute amplitude, α in (7a), to be obtained. Since we have to fit in order to obtain α, and the errors in W_b are large enough to significantly reduce the accuracy, we have chosen to fit the initial amplitude, α, the initial slope, β, and the Weber number, W_b. Having fitted the data, we then compare the fitted values and the measured values of each parameter. In addition, since we have chosen to fit the boundary conditions α and β, it does not matter where below the blade we choose to commence the fit. We therefore choose to start 2 mm below the blade position to ensure that we are outside the region of the disturbance [see equation (5) *et seq.*] and that therefore the system (7) should be completely valid. The numerically integrated system (7) was fitted to the data by means of a Levenburg–Marquardt nonlinear least squares algorithm.

Figure 5a shows a typical plot of measured signal, s [proportional to the slope according to equation (6)], together with a best fit where the blade was set at $x = 53$ mm (see figure 1). Figure 5b shows the corresponding amplitude and phase components of the measured signal as a function of curtain height together with their fits. The overlay of the data and fit are extremely good in both cases. The slight discrepancy at $x \approx 96$ mm is due to the crossing of small stationary waves initiated at the die corners. The accuracy of the comparison is therefore limited by systematic errors arising through the liquid sheet not being perfectly uniform. As stated above, to assess that the fitted parameters correspond to physically obtainable quantities we have chosen to plot, for all conditions examined, the fitted value of the initial signal against its measured value, Figure 6a, and the fitted Weber number, W_b, against its measured value, Figure 6b. It is quite clear that in each case the data lie on a 45° line

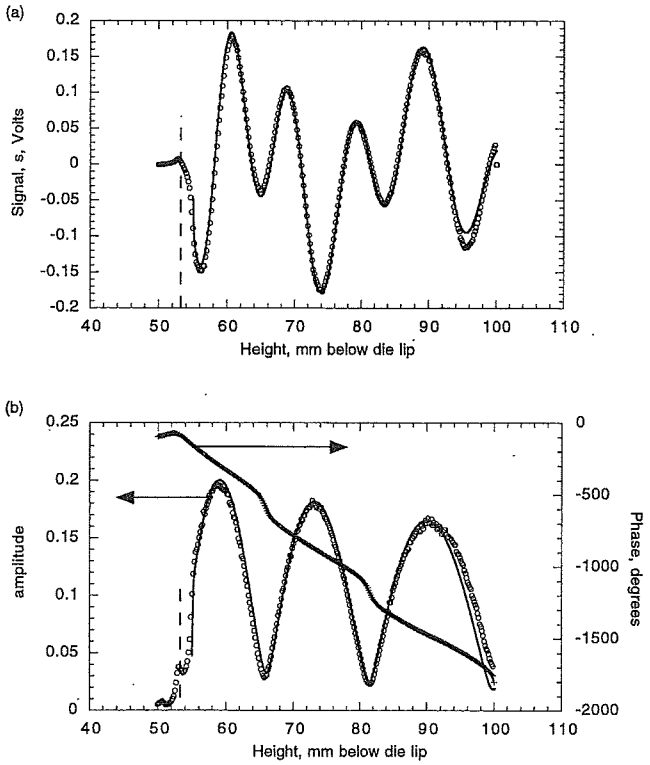

FIG. 5. Typical curtain data for $q=4.54\ \mathrm{cm^2/s}$, $\sigma=66.0\ \mathrm{mN/m}$, $\rho=1.2089\ \mathrm{g/cm^3}$ ($W_b=0.114$), and $\omega=440\ \mathrm{rad/s}$ (70 Hz). The electrostatic blade was positioned at $x=53$ mm as indicated by the dashed line. (a) The measured signal, s, together with the fit as a function of height below the die lip. (b) The same dataset plotted separately as amplitude and phase. The phase has been unwrapped to emphasise its continuous variation.

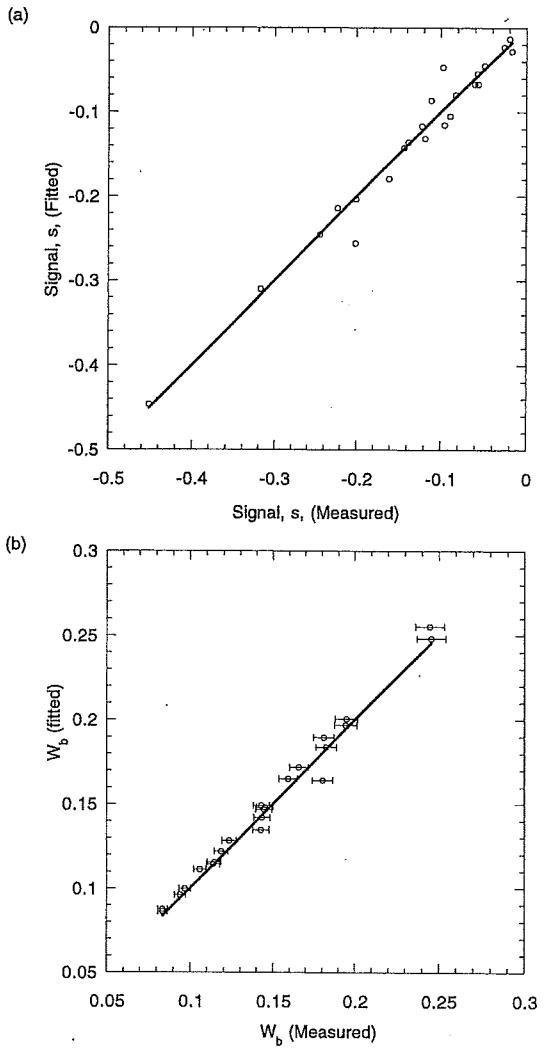

FIG. 6. Verification that fitted parameters correspond to measured quantities of the sinuous governing equation. Data are provided for a range of flow rates, $2.65\ \mathrm{cm^2/s}<q<4.71\ \mathrm{cm^2/s}$, frequencies 691 rad/s (110 Hz), 440 rad/s (70 Hz), and 251 rad/s (40 Hz), and blade heights ($33\ \mathrm{mm}<x_b<93\ \mathrm{mm}$). (a) A comparison of the real part of the measured signal corresponding to the slope of the liquid air interface and the fitted value. (b) The corresponding comparison of the measured and fitted value of Weber number, W_b.

through the origin indicating that the fitted parameters correspond to physically obtainable quantities. This then verifies that the governing equation correctly describes sinuous time-dependent disturbances propagating down the curtain and the resulting shape of the liquid–air interfaces.

The shape of the amplitude plot in Figure 5b implies a simple physical interpretation of the wave propagation. If we consider Lin's description[3] of two waves propagating at velocities,

$$c_r=u\pm c, \tag{10a}$$

where

$$c=\sqrt{\frac{2\sigma u}{\rho q}}, \tag{10b}$$

then at a given frequency two waves will propagate down the curtain, provided $u>c$. These two waves will linearly superpose and interfere leading to the nodes and antinodes observed in the amplitude plot. Furthermore, the distance between successive nodes will increase as the distance from the die lip increases reflecting the fact that the curtain is in free fall and therefore accelerating.

Figure 7 shows two plots from the extremes of the data range which have been analyzed to obtain Figure 6. For two waves propagating down the curtain according to (10), the wavenumbers, k_1 and k_2, can be expressed as

$$k_1=\frac{\omega}{u-c}, \quad k_2=\frac{\omega}{u+c}, \tag{11}$$

where ω is the angular frequency and the wavenumber $k=2\pi/\lambda$ with λ the wavelength. Thus the shorter of the two wavelengths will be contained in k_1. Figure 7a corresponds to the largest value of k_1 investigated and Figure 7b, the smallest. We can define a dimensionless wavenumber $\bar{k}=(kh)$, where h is given by (1b). Thus, Figure 7a corresponds to $\bar{k}=1.08$ under the blade and Figure 7b to $\bar{k}=0.167$ under the blade. The governing equation is only expected to be valid when $\bar{k}$ is small, i.e., significantly less than 1, however, it is clear that the governing equation is well able to fit both these sets of data. At significantly higher frequencies ($\omega>1400$ rad/s, $\bar{k}>2.16$), deviations from the governing equation are seen although it is difficult to unam-

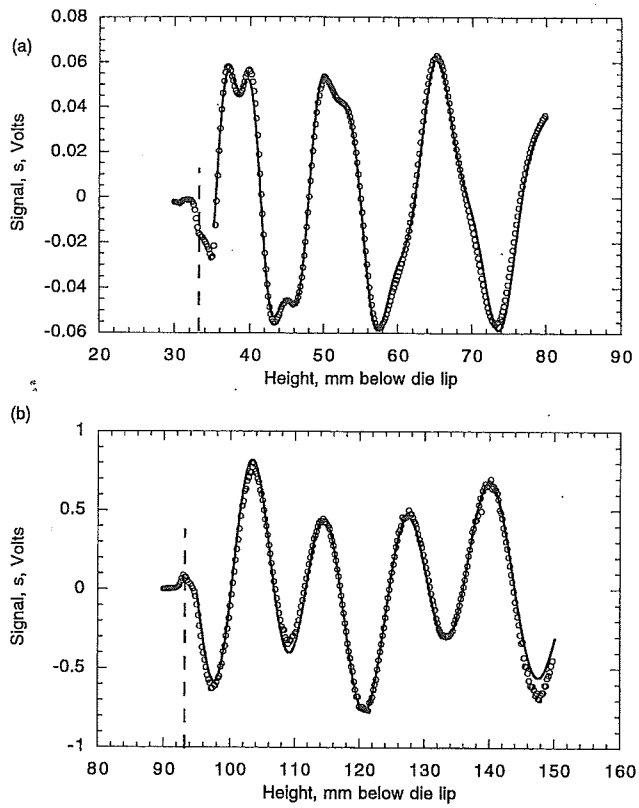

FIG. 7. A comparison of the data and the fitted governing equation at the extremes of the data range of figure 6. (a) Data and fit for $\bar{k}_1=1.08$, $W_b=0.143$, $\omega=691$ rad/s (110 Hz). (b) Data and fit for $\bar{k}_1=0.167$, $W_b=0.108$, $\omega=440$ rad/s (70 Hz). In both cases, the position of the electrostatic blade is indicated by a dashed line.

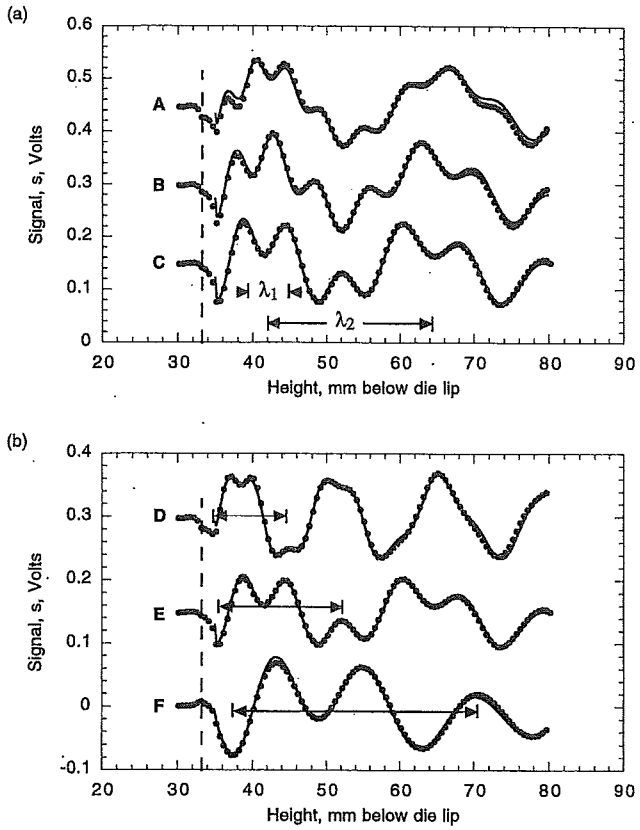

FIG. 8. The effect of the flow rate and the frequency on curtain shapes. The electrostatic blade position is indicated by a dashed line. In each plot the points are the data and the solid lines are the respective theoretical curves. (a) Variation of the measured curtain shape as a function of the flow rate for constant driving frequency, $\omega=440$ rad s^{-1} (70 Hz). Density $\rho=1.2089$ g/cm, surface tension $\sigma=66.0$ mN/m, and the blade height was 33 mm. Curve A, $q=2.65$ cm^2/s ($W_b=0.245$, $\bar{\omega}=9.58$); curve B, $q=3.56$ cm^2/s ($W_b=0.183$, $\bar{\omega}=11.7$); curve C, $q=4.54$ cm^2/s ($W_b=0.143$, $\bar{\omega}=13.7$). Approximate scales [$\lambda_1=(2\pi/k_1)$ and $\lambda_2=(2\pi/k_2)$] are also indicated. (b) Variation of the measured wave shape as a function of driving frequency for constant flow rate $q=4.54$ cm^2/s ($W_b=0.143$). curve D, $\omega=691$ rad/s (110 Hz); curve E, $\omega=440$ rad/s (70 Hz); curve F, $\omega=251$ rad/s (40 Hz). A characteristic length is indicated for each curve by a horizontal arrow; see the text for details.

biguously identify the point at which this occurs given the spatial resolution of the detection/excitation system.

Figure 8 demonstrates how the shape of the curtain varies as either the frequency is held constant and the flow rate, q, varied (Figure 8a) or the flow rate is held constant and the frequency varied (Figure 8b). Although these shapes exhibit a non-trivial behavior, it is instructive to consider a simplified view of the underlying physics. For a given frequency ω, there are two waves propagating in the curtain with differing wavenumbers according to (10). Thus we can express the superposition of the slopes of these waves as

$$\frac{\partial y}{\partial x}=a(x)\exp[i\omega t+k_1(x)x]+b(x)\exp[i\omega t+k_2(x)x], \tag{12}$$

where y is the displacement, $a(x)$, $b(x)$ are the amplitudes of the two waves, ω their frequency, and k_1, k_2 are given by (11). In Figure 8a, the underlying long wavelength periodicity corresponds to k_2, whereas the short wavelength component corresponds to k_1. In principle, changing the flow rate, q, will change both the wave speed c and the initial curtain velocity V. However, with our die design, the change in V over this range of flow rates leads to a negligible change in u in the region of interest. Consequently, since the driving frequency does not differ between the curves A, B, and C, the observed wavelength changes are essentially due to the wave speed c altering. In particular, as q increases (A to C) the wavespeed, c, decreases and therefore from (11) k_1 decreases and k_2 increases. That is, the long wavelength component ($\lambda_2=2\pi/k_2$) shortens its wavelength whereas the short wavelength component ($\lambda_1=2\pi/k_1$) lengthens its wavelength.

We note here that variation in the Weber number is accomplished through changes in the volumetric flow rate per unit width, q [see the definition of W_b in equation (9)], and this changes the starting velocity V [defined in (1a)] at the die. As indicated in (7b), the frequency is defined in terms of this scale. Thus, in dimensionless terms, our experiment cannot be viewed as for a "fixed frequency." The longer scale wavelength in Figure 8a is reduced in curve C compared with A (the bar in the figure is an approximate length); this may be partially accounted for by the increase in dimensionless frequency in curve C compared with curve A.

In Figure 8b, we have superposed a characteristic length, indicated by a bar, on each of the three curves. Compare the

curves D, E, and F; the difference is mostly a simple change in the overall length, i.e., although the relative amplitudes of the short and long wavelength components change, the general shape of the curves remain similar as the frequency is decreased, albeit with increased length. Again, this can be understood qualitatively from equation (12); both the wavespeed, c, and the liquid velocity, u, do not change between curves and thus the ratio of the wavelengths of the two components does not change [i.e., for these cases $k_1/k_2 = (u+c)/(u-c) = \text{const}$]. Therefore, as the driving frequency increases each component shortens its wavelength by the same proportion and the curves shorten along the x axis without changing their form. We note here that in dimensionless terms, the experiment in Figure 8b corresponds to a case where W_b is fixed and the dimensionless frequency is varied. Thus, all of the observed wavelength change is a result of changing the driving frequency alone.

IV. SUMMARY

By means of non-contact excitation and optical detection schemes, we have demonstrated that the time-dependent sinuous governing equation is valid. The excitation is a well defined local pressure disturbance ideal for probing the governing equations set out in Part 1. The detection system is extremely sensitive, the accuracy of our results being limited by the planarity of the liquid sheet generated in our experiment. We have demonstrated how the curtain shape varies with flow rate, driving frequency and blade position, the three independent parameters entering the governing equation.

ACKNOWLEDGMENTS

The authors would like to thank both A. Rankin and J. Marshall who made many of the measurements presented in this paper.

[1]D. S. Finnicum, S. J. Weinstein, and K. J. Ruschak, "The effect of applied pressure on the shape of a two-dimensional liquid curtain falling under the influence of gravity," J. Fluid Mech. **255**, 647 (1993).

[2]J. I. Ramos, "Planar liquid sheets at low Reynolds numbers," Int. J. Num. Methods Fluids **22**, 961 (1996).

[3]S. P. Lin "Stability of a viscous liquid film," J. Fluid Mech. **104**, 111 (1981).

[4]S. P. Lin and G. Roberts, "Waves in a viscous liquid curtain," J. Fluid Mech. **112**, 443 (1981).

[5]M. G. Antoniades, R. Godwin, and S. P. Lin, "A new method of measuring dynamic surface tension," J. Colloid Interface Sci. **77**, 583 (1980;).

[6]I. Balbaert, G. Bleys, and P. Joos. "Measurement of the dynamic surface tension in an asymmetric free-falling film," J. Colloid Interface Sci. **115**, 362 (1987).

[7]C. H. Sohl, K. Miyano, and J. B. Ketterson, "Novel technique for dynamic surface tension and viscosity measurements at liquid–gas interfaces," Rev. Sci. Instrum. **49**, 1464 (1978).

[8]V. Vogel and D. Möbius, "Resonance of transverse capillary and longitudinal waves as a tool for monolayer investigations at the air/water interface," Langmuir **5**, 129 (1989).

[9]K. Miyano, "Local mechanical properties of monomolecular films on water measured with a capillary wave probe," Langmuir **6**, 1254 (1990).

[10]S. J. Weinstein, J.-M. Baumlin, and J. Servant, "The propagation of surface waves in flow down an oscillating inclined plane," AIChE. J. **39**, 1113 (1993).

[11]A. Miyake, "Coating die," Japanese patent publication JP 48-34946A.

[12]LabVIEW is a graphical programming language developed by National Instruments specifically for instrument control, data acquisition, and analysis.